Available online at www.sciencedirect.com
SCIENCE DIRECT
Agricultural and Forest Meteorology 133 (2005) 119–139
AGRICULTURAL AND FOREST METEOROLOGY
www.elsevier.com/locate/agrformet

Comparison of temperature and wind statistics in contrasting environments among different sonic anemometer–thermometers

H.W. Loescher [a,*], T. Ocheltree [a], B. Tanner [b], E. Swiatek [b], B. Dano [c], J. Wong [d], G. Zimmerman [e], J. Campbell [f], C. Stock [g], L. Jacobsen [b], Y. Shiga [h], J. Kollas [i], J. Liburdy [c], B.E. Law [a]

[a] *Department of Forest Science, College of Forestry, Oregon State University, Corvallis, OR 97331, USA*
[b] *Campbell Scientific, Logan, UT 84321, USA*
[c] *Mechanical Engineering, Oregon State University, Corvallis, OR 97331, USA*
[d] *College of Oceanic and Atmospheric Sciences, Oregon State University, Corvallis, OR 97331, USA*
[e] *Applied Technologies Inc., Longmont, CO, USA*
[f] *R.M. Young Company, Traverse City, MI 49686, USA*
[g] *Gill Instruments Ltd., Lymington, Hampshire SO41 9EG, UK*
[h] *Kaijo-Denki, Tokyo 205-8607, Japan*
[i] *Metek GmbH, Elmshorn D-25337, Germany*

Received 10 March 2005; accepted 23 August 2005

Abstract

Sonic anemometers–thermometers (SATs) are robust instruments used in numerous research and analytical micrometerological studies. The accuracy and precision of the measured mean and turbulent fluctuations of wind speed and temperature are unknown across a range of ambient conditions and among different model SATs. Here, we compared quantities from eight different model SATs: (i) mean temperature ($\overline{T_s}$) in an acoustically isolated chamber, (ii) mean vertical wind speed ($\overline{w_s}$) in a low-speed wind tunnel, and (iii) wind statistics with data collected over a research field. Potential differences in buoyancy flux ($\overline{w'T'}$) due to different responses among SATs to changes in air temperature were also examined. The $\overline{T_s}$ response from each model SAT to air temperature departed from a 1:1 relationship across all, or part, of the range in tested temperatures. $\overline{w_s}$ from all SATs did not behave 1:1 to an independent measure of vertical wind speed using a hot-film anemometer, and there were consistent patterns based on the physical design of the SAT. The observed differences in σ_w^2 and σ_T^2 among SATs and their potential to affect scalar fluxes are discussed. Large variability was observed in wind statistics among SATs in field conditions. Uncertainty in $\overline{w'T'}$ among sensors due to their different responses to $\overline{T_a}$ for each 15-min averaging period ranged −23.1 to +16.1%, and range from −1 to +8% when averaged over ∼940 15-min periods. Use of SAT derived data are discussed for: (i) estimating fluxes, advection, and the WPL term, (ii) comparison of data from multiple SATs in an individual study, and (iii) temporal and spatial scaling or comparisons of flux estimates that were derived from different model SATs.

Keywords: Sonic anemometer; Sonic temperature; Wind tunnel; Comparison; Uncertainties

* Corresponding author. Tel.: +1 541 737 8020; fax: +1 541 737 1393.
E-mail address: hank.loescher@oregonstate.edu (H.W. Loescher).

0168-1923/$ – see front matter © 2005 Elsevier B.V. All rights reserved.
doi:10.1016/j.agrformet.2005.08.009

1. Introduction

Three-dimensional sonic anemometers–thermometers (SATs) are robust instruments based on speed-of-sound (SOS) measurements and are integral in advancing our knowledge of turbulent flows (Mahrt et al., 2000; Paw et al., 2000; Katul et al., 1999; Lee, 1998), surface energy balance (Burba and Verma, 2001; Katul et al., 1995), and scalar fluxes (Hollinger et al., in press; Loescher et al., 2003; Law et al., 2001; Clark et al., 1999; Goulden et al., 1996). All these areas of research rely on accurate and precise measurements of mean and variance of (time-averaged) wind velocities and SOS derived temperature. This is particularly true in determining scalar fluxes using the eddy covariance (EC) technique, where precision is needed to determine the: (i) turbulent fluctuations defined by the deviations from a mean quantity (cf. Loescher et al., submitted for publication; Baldocchi, 2003), (ii) coordinate framework (Lee et al., 2004; Wilczak et al., 2001), (iii) mean velocities to estimate vertical and horizontal advection (cf. Lee, 1998; Paw et al., 2000), and (iv) Webb, Pearman and Leuning (WPL) term that accounts for errors (unit conversion) introduced by fluctuations in water vapor density and temperature which are not associated with the net transport of CO_2 (Luening, 2004; Massman, 2004).

Yet, some uncertainties in the EC technique stem from flows not fully accounted for within and below the sensor-field. This has led researchers to re-examine how the conservation equation has been applied to this technique (cf. Loescher et al., submitted for publication). Bias in flux due to tilt errors (e.g., Lee, 1998; Lee et al., 2004), improper coordinate rotation (cf. Lee et al., 2004), vertical (Lee, 1998) and horizontal advection (Paw et al., 2000) are largely theoretical arguments and rely on our ability to estimate a *true mean vertical velocity*. In practice, the implementation of many advocated corrections may introduce more variability in flux estimates from one averaging period to the next (i.e., run-to-run variability), and at best provide constraints on flux estimates only at longer time integrals. Additional systematic bias in SAT-derived estimates can also occur within sites where multiple EC systems are operated, and when comparing results among different research sites.

Kaimal and Gaynor (1991) found that sonic temperature (T_s) ≈ virtual temperature (T_v) once they had accounted for the effects of water vapor, as measured by a k-probe SAT (Table 1). Hollinger et al. (pers. comm.), however, found a large variation in T_s among different models of SATs, and it is unclear if this variation was due to systematic or random error. Researchers often adjust their T_s to T_v by applying an offset determined empirically through regression analysis with independently measured (aspirated) air temperatures and humidity estimates. This approach is only valid if the SAT response is linear across a range of temperatures and humidity, and the function of each transducer is independent of changes in temperature and humidity.

Using R2 and R3 SATs (cf. Table 1), Van der Molen et al. (2004) found that vertical wind velocities were underestimated dependent on large angles of attack and wind direction, and by applying empirical sine corrections to their data found that scalar covariances were also underestimated by 5–15%. Gash and Dolman (2003) argue that winds with large angles of attack carry a large percentage of the total turbulent flux and the inability of SATs to measure these flows contribute towards poor energy balance closure at many forested sites.

Each SAT manufacturer employs a different physical configuration and electronic processing each with their own uncertainty. All account for flow distortions and transducer shadow errors that are unavoidable (cf. Kaimal et al., 1990; Wyngaard and Zhang, 1985). But specific processing routines, internal averaging, filtering, and aliasing of data are generally proprietary features, the effects of which are not available to general users. Factory calibration methods also differ, some rely on modeled relationships, others on empirically derived ones. In all cases, the ensemble of processing codes and the ability to account for flow distortions differ among different model SATs, and likely has direct bearing on the precision of the mean and variances of wind velocities and sonic temperature used in the EC technique.

The objective of this study is to examine how the response of each model of SAT differs to changes in: (i) temperature in an acoustically isolated and climate controlled chamber and (ii) the vertical wind statistics in a controlled wind tunnel. A second objective was to compare the vertical wind and temperature variances from each model SAT in field conditions.

2. Methods

2.1. Theoretical considerations

The SOS measurements were made between three pairs of send-and-receive transducers. Paired transducers are either arranged in orthogonal or non-orthogonal configurations and internal (and proprietary) software

Table 1
A list of the SATs used in this study, configurations are Y and P for yoke-style and post-mounted sonic volume, respectively, and NO and OT is non-orthogonal and orthogonal transducer array. If flow from all angles are acceptable for SAT measurement, *none* is noted for the acceptance angle

Manufacturer	Model	Configuration	Resolution		Path length (m)	Acceptance angle, $^{\circ}\theta_A$	Sampling, output rate (Hz)	Transducer face area (cm^2)
			Wind speed	temperature				
			$m\ s^{-1}$	$^{\circ}C$				
TSI Inc., Minneapolis, MN	IFA-300	3-D hot film	0.001	na	na	None	na	na
Applied Technologies Inc. Longmont, CO	a-Probe	Y, NO	0.01[a]	0.01	12.0	None	200, 40	0.785
Applied Technologies Inc. Longmont, CO	k-Probe	Y, OT	0.01[a]	0.01	15.0	None	200, 40	0.785
Campbell Scientific Inc., Logan, UT	CSAT-3	Y, NO	0.001[b]; 0.0005[c]	0.002	10.0	None	60[d], 10 or 20	0.315
Gill Ltd., Hampshire, UK	R3	P, NO	0.01[e]	0.01	15.0	±20°	na	na
Kaijo-Denki, Tokyo, Japan	DA-600 (TR61A)	Y, NO	0.005	0.025	20.0	±45°	10, 10	0.7
Kaijo-Denki, Tokyo, Japan	SAT-550	P, NO	0.01	na	10.0	±20°	50, 50	na
Metek GmbH, Elmshom, Germany	USA-1	P, NO	0.01	0.01	17.5	None[g]	na	na
R.M. Young Inc., Traverse City, MI	RM-81000	P, NO	0.01[f]	0.01	15.0	±20°	140, 4–32	0.69

[a] Median filters were applied.
[b] For this study, the CSAT was not equipped with the rain upgrade for u_x and u_y.
[c] For u_z.
[d] Oversample mode.
[e] R3 signals are internally digitized in bins that exclude data in every multiple of 7 $m\ s^{-1}$, then a smoothing algorithm is applied (C. Thomas and T. Foken, personal communication).
[f] This sensor has a 0.01 $m\ s^{-1}$ threshold for vertical velocities, below which, wind speeds are set to zero. In this study, the threshold was set to its resolution value of 0.01 $m\ s^{-1}$.
[g] Metek now report an acceptance angle of ±45° for the USA-1.

determines the vector quantities. The *difference* in time-of-flight between each pair of transducers are a function of wind speed, and estimates of air temperate (measured in the vertical axis) are based on internal *averaged* time-of-flight measurements, such that,

$$c_a = \underbrace{\sqrt{\frac{RT_a}{M_a}\frac{C_p}{C_v}}}_{\text{I}} = \underbrace{\sqrt{\left[\frac{d}{2}\left(\frac{1}{t_{ba}}+\frac{1}{t_{ab}}\right)\right]^2 + U_n^2}}_{\text{II}} \quad (1)$$

where c_a is the speed of sound through dry air (m s^{-1}), R the ideal gas constant (8.3144 kg m^2 mol^{-1} K^{-1} s^{-2}), T_a the temperature of dry air (K), M_a the molecular weight of dry air (kg mol^{-1}), C_p and C_v the specific heats of dry air at constant pressure and volume, respectively (1004 and 717 J kg^{-1} K^{-1}; Fleagle and Businger, 1980), d the sonic path length (m), t the transit times between the send and receive transducers a and b (s), and U_n is the component of the wind velocity that is normal to the sonic path length (m s^{-1}). In Eq. (1), term I estimates the SOS based on the physical attributes of air, and term II is the logic employed with sonic anemometers. This means that under non-steady state conditions the transit times are also not constant due to changes in air density, but also dependent on the secondary effects of temperature on the piezoelectric material in the sonic transducer. Hence, errors in SAT-derived estimates can be introduced by the use a fixed time constant to transit between t_{ab} and t_{ba}. All the SATs used in this study also account for crosswind effects in their internal processing, thus we did not need to apply the crosswind corrections presented in Liu et al. (2001) because it amounts to double accounting.

Measuring the SOS in the natural environment includes the influence of water vapor, which also has the ability to retain sensible heat. Virtual temperature is the temperature of dry air with the same density and pressure of ambient moist air, such that;

$$T_v = T_a\left(1 + 0.38\frac{e}{P_a}\right) \quad (2)$$

where T_v is the virtual temperature (K), e the partial pressure of water vapor in air (Pa), and P_a is the atmospheric pressure (Pa, Eq (A.2), Appendix A). Use of T_v is appropriate in determining many boundary-layer estimates, including stability parameters, flows due to buoyancy, and turbulent kinetic energy budgets (Kaimal and Gaynor, 1991).

Sonic temperature is,

$$T_s = \underbrace{\frac{C_v}{C_p}\frac{M_a c_a^2}{R}}_{\text{I}} = \underbrace{\frac{d^2}{1612}\left[\frac{1}{t_{ba}}+\frac{1}{t_{ab}}\right]^2}_{\text{IIA}} + \underbrace{\frac{U_n^2}{403}}_{\text{IIB}} \cong \underbrace{T_v - \left(0.06\frac{T_a}{P_a}\right)e}_{\text{III}} \cong \underbrace{\frac{C_v}{C_p}\frac{M_a c_w^2}{R}}_{\text{IV}} f \quad (3)$$

with $T_s < T_v$,

where T_s is the sonic temperature (K), c_w the SOS in moist air, and f is a reduction factor to account for the effects of water vapor on sonic thermometry. By reconfiguring Eq. (1), term I is theoretical T_s in dry air. Term II depicts how the SAT also estimates T_s theoretically, but which has the effect of water vapor inherent in the data. Schotanus et al. (1983) have elegantly presented means to account for all the crosswind effects on T_s, i.e., term IIB. If T_a and P are constant during a measurement period, then T_s can be estimated by a theoretical term III that accounts for the effects of water vapor (Kaimal and Gaynor, 1991). Term IV is the measured T_s by the SAT in moist air with a reduction factor (i.e., $f < 1$) to describe the effects of water vapor, making f only accurate to ~0.02 K and has the same affect as rounding to 403.

2.2. Acoustically isolated chamber

The relationship between $\overline{T_s}$ and $\overline{T_a}$ (time-averaged indicated by the overbar) was investigated from nine different models of SATs (Table 1). Ideally, a population of each model SAT should be used to test its response to different environmental conditions. Because of the impracticality of this approach, each manufacturer instead provided a 'best-calibrated' sensor to this study. An acoustically isolated chamber ~1.2 m × 0.6 m × 0.6 m (inner measurement) was constructed, covered on the outer surface by 5 cm foam insulation, and lined on the inside with a 2.6 cm layer of acoustically isolating foam. Temperature of the chamber was controlled by passing ethylene glycol (antifreeze grade) through 18 m of 1.3 cm i.d. tubing coiled inside the chamber, between the chamber wall and acoustical foam. A refrigerated and heated circulator (Model 2096, Forma Scientific, Marietta, OH) was used to heat, cool and flow the ethylene glycol through the chamber.

To accurately measure SOS under steady-state conditions, care was given to ensure that the environment inside the sealed chamber was isothermal, with no significant air movements or temperature gradients. The

temperature distribution inside the chamber was measured using six thermocouples (copper tungsten, 24 AWG) placed equidistant around the inside, and two platinum resistance thermometers (PRTs, Model 810 with linearizer OM5-IP4-100C, Omega Inc., Stamford, CT) placed above and below the sonic volumes. Steady-state conditions were met when no two thermocouples differed by more than 0.2 °C (B. Tanner and L. Jacobsen, personal communication, Campbell Scientific Inc.), and the difference between the PRTs was <0.1 °C. The PRTs were calibrated in-house using ice water (0 °C), water vapor (100 °C), and a gallium cell (29.77 °C) according to NIST protocols, and remained inside the chamber throughout testing as the independent measure of $\overline{T_a}$.

SATs were tested across a range of temperatures from ~0 to 30 °C at 2 °C increments. Two SATs were placed inside the chamber simultaneously, and oriented so that the yoke or post passed through the side of the chamber eliminating any electronic induced heat that may create convective currents inside the chamber. Data from the PRTs were collected with a datalogger (Model CR5000, Campbell Scientific Inc., Logan, UT). SAT data were collected digitally through a serial port by a laptop computer, except the Kaijo-Denki SAT-550 (as recommended by the manufacturer) in which data were collected with the CR5000 datalogger.

Allan's (1966) variance was used to determine an appropriate averaging time that minimized the variability due to signal noise (at shorter timescales) and drift in steady-state environmental conditions (longer timescales, cf. Werle et al., 1993). The $\overline{T_s}$ from the CSAT-3 were used for this Allan's variance analysis and because it had been classified as an analytical research SAT (Foken and Oncley, 1995; M. Mauder, personal communication) was assumed its signal:noise ratio was representative of all other SATs. All SATs were subject to the same changes in environmental (room) conditions.

T_s was not corrected for the influences of e in the chamber because all SATs and PRTs were subject to the same and consistent low value of e during the comparison, and the linear correction would not affect least squares estimates (cf. Eq. (2)). This logic was applied to the remainder of this study.

2.3. Wind tunnel

The flow distortion in $\overline{w_s}$ was estimated from the nine different SATs under steady-state conditions in a low-flow wind tunnel. We assumed the maximum flow distortion from post-style SATs would occur as flow passed from the cylindrical base towards the sonic volume, i.e., upward welling flows in the natural environment. We also assumed that the maximum flow distortion would occur close to the manufacturer's acceptance angles ($^{\circ}\theta_A$, Table 1; Shimizu et al., 1999). For this reason, the mean flow of the wind tunnel was aligned with M which was determined by being 5° within $^{\circ}\theta_A$ ($^{\circ}\theta_B$, Fig. 1), such that,

$$\text{If } {}^{\circ}\theta_A > 0, \quad \text{then } {}^{\circ}\theta_B = 90^{\circ} - ({}^{\circ}\theta_A - 5^{\circ}) \tag{4a}$$

$$\text{If } {}^{\circ}\theta_A = \text{none}, \quad \text{then } {}^{\circ}\theta_A = 90^{\circ} \quad \text{and} \quad {}^{\circ}\theta_B = 90^{\circ} - ({}^{\circ}\theta_A - 5^{\circ}) \tag{4b}$$

with the mean flow moving from the base (bottom) towards the sonic volume. Because each yoke-style SAT was symmetric, we assumed the associated flow distortions in $\overline{w_s}$ were relatively the same regardless of the direction in mean flow, i.e., flows from the top-down or bottom-up. But for consistency sake, they were positioned with the bottom of the sensor facing mean flow. The design of post-style SATs requires vertical stanchions to support the upper array of sonic transducers. We also estimated any additional flow distortion caused by these stanchions with the same methodology described above with and without the vertical stanchions in-line to the mean wind flow.

The wind tunnel was a closed, oval-loop that could accommodate low wind speeds. The overall size was

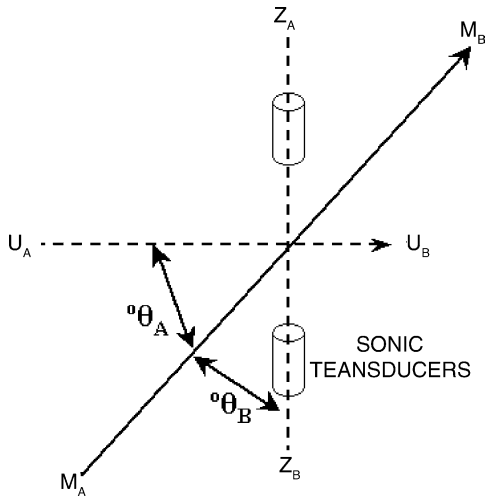

Fig. 1. A 2-D graphic representation of Eqs. (4a) and (4b). U and Z are the horizontal and vertical axis of a SAT, M is the vector aligned with mean wind flow, and $^{\circ}\theta_A$ is the manufacturer's acceptance angle (Table 1).

9.2 m × 5 m × 2.5 m ($L \times W \times H$) with a test section ~3.8 m × 1.8 m × 1.8 m. Flow was controlled by a 1.6 m variable speed, variable pitch propeller, powered by a 20 hp motor. Prior to entering the test section, wind was forced into laminar flow by fine-mesh screen, honeycombs, and straighteners before passing through the contraction cone of the tunnel. The turbulence intensity within the test section was <1%.

SATs were placed inside the wind tunnel along with a 3-D hot-film anemometer (Model IFA300, TSI Inc., Shoreview, MN) as the independent measure of vertical wind speed ($\overline{w_{hf}}$). Hot-film data were collected using the self-optimizing bridge circuit (Model 183150, TSI Inc.) that was specifically designed for closed-loop wind tunnels and to account for the effect of temperature changes on wind velocity measurements. The tunnel temperatures did not change more than 0.4 °C during any 30-min sampling period. Each anemometer was placed in the center of the cross-section of the wind tunnel to be far away from internal boundary layers near the tunnel walls. Care was given to minimize any flow distortion caused by adjacent instrumentation. All mounting hardware was downwind (behind) the sonic volume for yoke-style SATs and the hot-film sensor. Post-style SATs had custom mounts fabricated that matched the outside circumference of their respective cylindrical base and all other supportive mounting was beneath and downwind (behind) the sonic volume. In all cases, the mounting was positioned such that there were no physical obstructions between the sonic volume and the free-flow environment of the wind tunnel. The lateral separation between the SAT and hot-film anemometer was ~20 cm relative to the flow in the tunnel. Because the cylindrical body of the hot-film anemometer was only 3.2 mm, we assumed mean flow was re-established within a few cm from the body, eliminating or minimizing any lateral flow distortions caused by the hot-film anemometer in the sonic volume. The hot-film anemometer was also aligned to measure the same vertical wind velocities at the same attack angle as needed by each SAT. The hot-film anemometer was calibrated in an air velocity calibrator (Model 1129, TSI Inc.) to manufacturer's specifications (0.01% of full scale) across all acceptance angles and for wind speeds ≤1 m s^{-1}.

Because flows in the wind tunnel become variable and non-steady state at velocities <0.2 m s^{-1}, and because most vertical wind velocities in natural environments are <1.0 m s^{-1}, three mean wind velocities in the wind tunnel were used to test $\overline{w_s}$ for each SAT, 0.2, 0.5, and 1.0 m s^{-1}. The measured $\overline{w_s}$ was then expected to differ among each SAT depending on the attack angle used. The 20 Hz data from the hot-film anemometer were triggered synchronously with the SATs. The $\overline{w_s}$ from the Kaijo-Denki SAT-550 were used in an Allan's variance analysis to estimate the optimal averaging and we assumed its signal:noise ratio was representative of all other SATs.

2.4. Field experiment

A comparison of vertical wind velocities and sonic temperature were made under in situ turbulent field conditions among the SATs (not including the hot-film anemometer). Data were collected from September 28 to October 8, 2004, at the Oregon State University Hyslop agronomic research site, Corvallis, OR (44°38′N, 123°12′W, m.a.s.l. 68.6 m).

All SATs were mounted on the same triangular tower, on one of two booms that extended from either side. The configuration of SATs on the tower was designed to minimize any flow distortion, and all sonic volumes faced into the mean path of horizontal wind at 43° (with declination). All post-style SATs were mounted on one side of the tower with the base of the boom at ~2.25 m. All yoke-style SATs were placed on the opposite side of the tower on the second boom. Care was given so that the center of the z-axis from all sonic volumes was aligned and level at the same 2.75 m a.g.l. The distance between vertical centerlines of the two SATs on either end of each boom was 3.3 m. Lateral placement of all SATs on each boom is depicted in Fig. 2 (cf. Kristensen et al., 1997). All sonic data were digitally collected at 20 Hz (with the exception of the Kaijo-Denki SAT-550 which only outputted data at 50 Hz) through a 32-bit, 8-port RS-232 hub at 9800 baud (Model ESC-100-D9, Quatech, Hudson, OH). No triggering was used.

The fetch was >800 m over flat terrain, and was covered with low density of grasses and forbs (~50 plants m^{-1}) that were established in 2004 from a natural seed bank. The mean vegetative canopy height during the sampling period was ~0.05 m. Meteorological data collected at Hyslop research site by the Oregon Climate Service (http://www.ocs.oregonstate.edu) reported that the air temperatures ranged 6.26–25.67 °C and daily averages ranged 12.7–17.6 °C, relative humidity ranged 79–93%, net radiation ranged 3.4–11.8 MJ d^{-1}, and horizontal wind speed 0–6 m s^{-1} with >1/2 of the sampled time having wind speeds <2 m s^{-1}.

Raw data were processed with EdiRe software (R. Clement, University of Edinburgh, UK). The optimal averaging period was determined using integrated cospectra (ogives, cf. Loescher et al., submitted for publication) of $\overline{w'T'}$ and $\overline{w'u'}$ (Eq. (A.1), Appendix A).

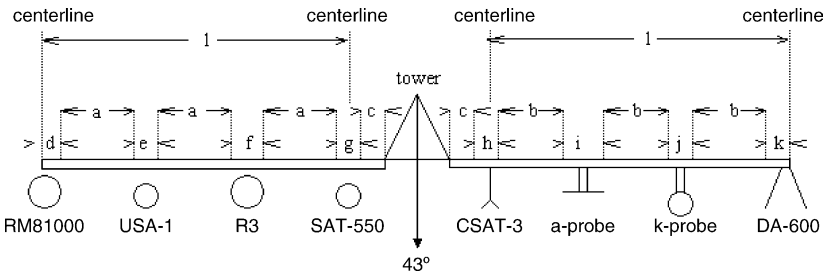

Fig. 2. A drawing that depicts the lateral placement of each SAT on the booms during the field experiment at the Hyslop agronomic research site, Corvallis, OR, where *a* to *l* are 80, 86, 30, 17, 32, 27, 24, 12, 18, 26, 23, and 330 cm, respectively.

Second-order statistics (i.e., covariances) were calculated using a block average as per recommended by AmeriFlux Steering Committee (cf. Standardization of Flux Analysis and Diagnostics Meeting, Corvallis, OR, August 2002). By using a block average over other methods of mean removal (e.g., Reynolds averaging, linear detrending, and running average), places more of the fluctuations from a mean (from each averaging period) into the measured turbulent environment. Outliers were determined if a data point was >6 S.D. from the time-averaged mean (with a maximum of four data points in succession), and replaced with the previous data point. For each averaging period, $\overline{T_s}$, σ_T^2, $\overline{w_s}$, σ_w^2, $\overline{w'T'}$, and $\overline{w'u'}$ were calculated in a non-rotated and 2-D rotated coordinate framework, where σ_x^2 is the sampling variance and x denotes the scalar T or vector w. Horizontal wind statistics ($\bar{u}$ and σ_u^2), stability parameter (ς, Eq. (A.3), Appendix A), spectra and cospectra, and stationarity for $\overline{T_s}$ were also calculated in the 2-D coordinate framework. Stationarity was estimated using three 5-min time segments for each averaging period. Data were removed when: (i) wind directions were ±45° outside from the SAT orientation, (ii) precipitation occurred, and (iii) stationarity in $\overline{T_s} > 25\%$. Comparisons of each time-averaged wind statistic were made using first-order regression between each SAT to the response of the CSAT-3 among stability classes. The CSAT-3 was used here because it is used by the DOE AmeriFlux QA/QC laboratory as their network standard and it is the most frequently used SAT throughout the AmeriFlux network, and should not be taken as a direct endorsement of this sensor as an absolute standard.

To determine if the potential differences in $\overline{T_s}$ observed in the acoustically isolated chamber affect buoyancy flux estimates ($\overline{w'T'}$, Eq. (A.3), Appendix A), the response function (third-order polynomial) found between each SAT estimated $\overline{T_s}$ and PRT was universally applied to the same, standard time series. We used the 20 Hz time series data collected by the CSAT-3 in the Hyslop field test. These data were back-corrected to match the mean temperature response of the PRT (referred to as $\overline{w'T'_{prt}}$), then the response function in $\overline{T_s}$ from each SAT was applied to this time series (referred to as the modeled time series, $\overline{w'T'_{mod}}$), including the response function found in the CSAT-3 chamber data. All of the data in this in situ field test were within the temperature range used in the chamber experiment, increasing our confidence in $\overline{w'T'_{mod}}$. Estimates of $\overline{w'T'_{prt}}$ were subtracted from $\overline{w'T'_{mod}}$ and the percent difference between these two estimates was expressed from each SAT for each 15-min averaging period. Data were filtered using the above-mentioned criteria and presented by stability class, unstable ($\varsigma < -1.0$), slightly unstable ($-1 < \varsigma < -0.06$), near neutral ($-0.06 < \varsigma < 0.02$), and stable ($\varsigma > 0.02$).

3. Results

3.1. Acoustically isolated chamber

The effects of *e* were minimal, atmospheric pressure ranged and relative humidity ranged 3 kPa and 46–50%, respectively, resulting in <0.02 °C uncertainty across the range of measured $\overline{T_a}$. The optimal averaging time was 100 s for data collected in both the chamber and the wind tunnel (Fig. 3), resulting in a minimum of 18 averaging periods for each 30-min period of data collected. The signal-to-noise ratios did not vary more than 1.4× among SATs, even though the $\overline{T_s}$ response from each model SAT to $\overline{T_a}$ departed from a 1:1 relationship across all, or part, of the range in tested temperatures (Fig. 4). Most notably were the RM-81000 with a real temperature depression between 5 and 10 °C but within manufacturer's specifications (i.e., ±2 °C), and both ATI probes once the chamber temperatures were outside its calibrated range (Fig. 4A). The Campbell CSAT-3, Gill R3, and Kaijo-Denki SAT-550 $\overline{T_s}$ also departed from a 1:1 relationship at both ends of the temperature range tested (Fig. 4B). Heating the

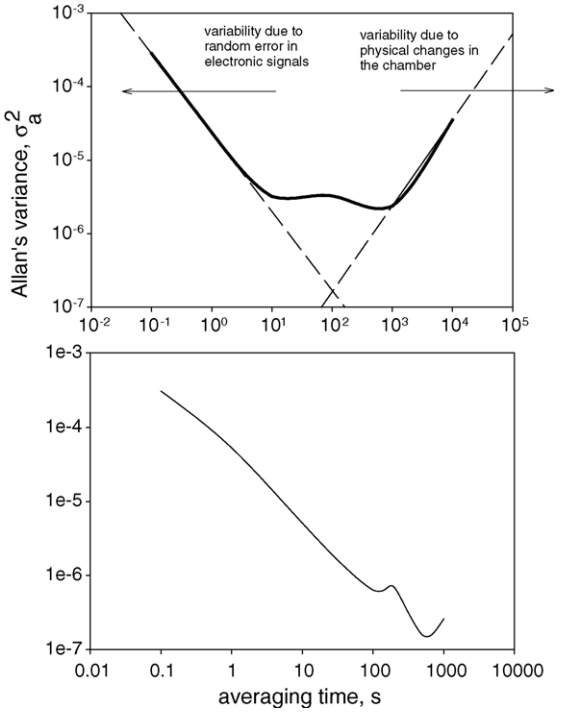

Fig. 3. Allan's variance for (A) 30-min sonic temperature data from the CSAT-3 and (B) 1 h of 0.5 m s^{-1} vertical wind speed data from the Kaijo-Denki SAT-550. Because the data show two equally low variances, two lines were extended through both slopes to determine the averaging period with minimal variability due to electronic processing and physical changes in the chamber.

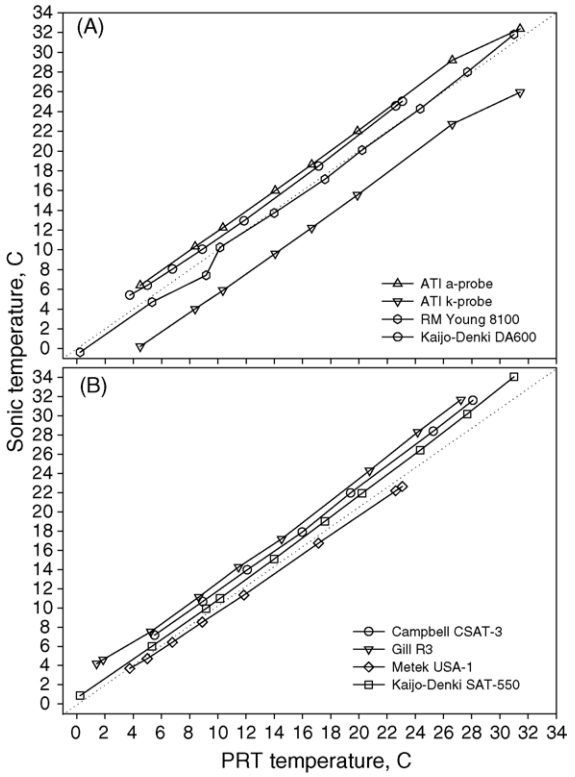

Fig. 4. Mean temperature response from each model SAT compared to platinum resistance thermometers (PRT) in a temperature controlled chamber. The coefficient of variation from PRT and SAT measurements were approximately the same, followed the same trends through the temperature range, and for temperatures >4 °C were <0.01. The two panels are for clarity.

chamber to the full range of temperatures could not be achieved when the Kaijo-Denki DA-600 and Gill R3 sensors were tested. Even though, all the SAT bodies were placed outside the chamber to prevent any instability from forming, we noticed that the RM Young 81000 emitted a large amount of heat; when the whole sensor was placed in the chamber, a 5 °C temperature differential was measured. The bodies of the Metek USA-1 and Kaijo-Denki SAT-550 were also noticeably warm to the touch. In the case of the USA-1, this observation seems anomalous to the product literature stating the sensor only consumes 2.5 W of power (i.e., all sensor heating was turned off).

The variance in sonic temperature, σ_T^2, did not differ among the range in tested temperatures. $\overline{w_s}$ ranged ± 0.01 m s^{-1} across the range in tested temperatures among most SATs, and was below manufacturers specifications. The two exceptions were the CSAT-3 and USA-1 SATs with $\overline{w_s}$ that ranged ± 0.02 m s^{-1} across the range in tested temperatures and with significant regressions, $y = 0.00178\overline{T_a} + 0.05$, $R^2 = 0.80$ and $y = -0.00145\overline{T_a} + 0.02$, $R^2 = 0.42$, respectively. The response of σ_w^2 from the k-probe, R3 and SAT-550 was linear to $\overline{T_a}$, $y = -9e^{-7}\overline{T_a} + 7e^{-6}$, $R^2 = 0.81$, $y = -9e^{-0}\overline{T_a} + 1e^{-6}$, $R^2 = 0.52$, and $y = 3e^{-6}\overline{T_a} - 2e^{-6}$, $R^2 = 0.61$, respectively.

3.2. Wind tunnel

The $\overline{w_s}$ from all SATs did not compare well to a 1:1 with $\overline{w_{hf}}$ (Figs. 5 and 6), but there were consistent patterns within each style of SAT (post versus yoke). Because of the limited acceptance angles of post-style SATs (due to the physical geometry of the instruments) and the ability of the wind tunnel to maintain constant flow conditions at low velocities, the range of tested vertical velocities differ between these post-style and the other SATs with no rejection angle. The DA-600 and USA-1 responses were linear, but the slopes were significantly different from unity, $y = 0.78(x) - 0.01$, $y = 0.66(x) + 0.18$, respectively (Fig. 5). The R3 also behaved linearly but only when the mean vertical velocities were not distorted by the stanchions, $y = 0.71(x) + 0.04$ (Fig. 5A). All post-style SATs

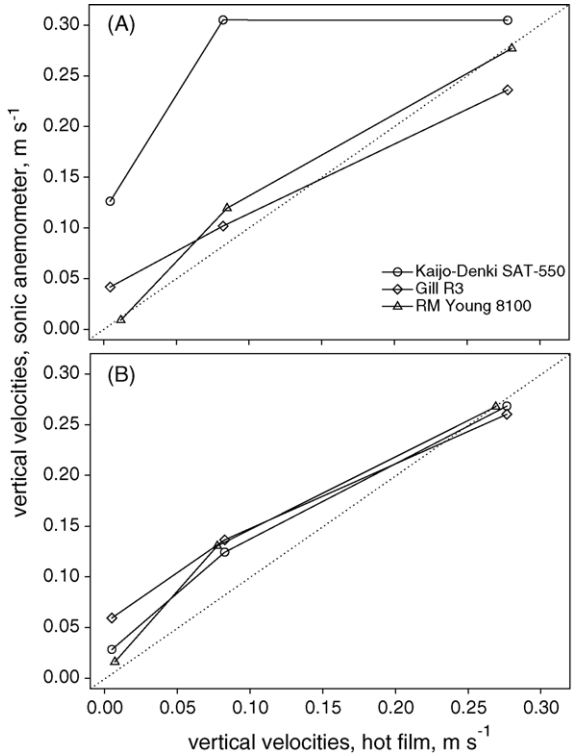

Fig. 5. Mean vertical wind velocities from the post-style SATs compared to hot-film measurements in a wind tunnel. Sonics were placed inside the wind tunnel 5° within the manufacturer's acceptance angles for the vertical component. Because post-style SATs have vertical stanchions to support the top set of transducers (A) is positioned so there is no flow distortion caused by the stanchions and (B) the stanchions are directly in the mean flow path. The coefficient of variation from the hot film and SATs were approximately the same, followed the same trends through the range of velocities and were generally <0.001.

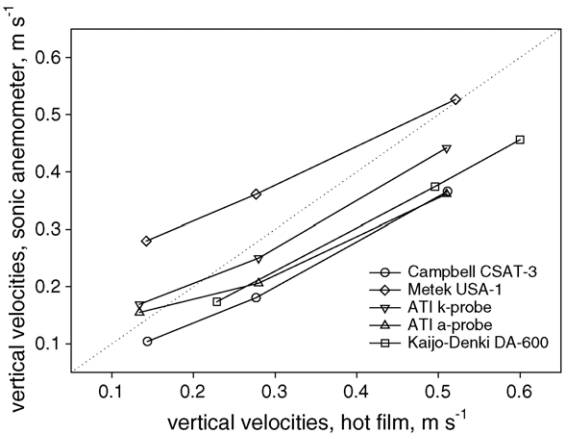

Fig. 6. Mean vertical wind velocities from the yoke-style SATs compared to hot-film measurements in a wind tunnel. Sonics were placed inside the wind tunnel 5° within the manufacturer's acceptance angles for the vertical component. The coefficient of variation from the hot film and SATs were approximately the same, followed the same trends through the range of velocities and were generally <0.001.

demonstrated increased vertical velocities at $\sim$0.08 m s^{-1} (Fig. 5). Most notable was the SAT-550 when there was no flow distortion associated with the stanchions (Fig. 5A). For flows that passed through the stanchions, the R3, SAT-550, and RM-81000 $\overline{w_s}$ converged to a 1:1 relationship to $\overline{w_{hf}}$ at >0.2 m s^{-1}. Conversely, the a-, k-probe and CSAT-3 yoke-style SATs showed decreased vertical velocities at $\sim$0.28 m s^{-1} (Fig. 5). More recent versions of the USA-1 restrict $^{\circ}\theta_A$ to $\pm$45°, and when tested with a $^{\circ}\theta_B$ = 25°, $\overline{w_s}$ from the USA-1 diverged from a 1:1 with $\overline{w_{hf}}$ across part, or all of the range in $\overline{w_s}$ (Appendix C).

3.3. Field experiment

A representative time series for T_s and w from each SAT show that not each sensor measures the same turbulent features (Fig. 7). For example, the ramp-like structures in T_s measured by some SATs and not others (as indicated by solid sloped lines between 0 and 20 s in Panel A, Fig. 7), and the sharp decrease in temperature at the end of a convective cell (as indicated by arrows, Panel A, Fig. 7). The decrease in temperatures was often accompanied by downward motions (as indicated by arrows, Panel B, Fig. 7). Other anomalous behavior was also observed such as the flattened peaked structures in the USA-1 data (as indicated by dotted lines in Panel A, Fig. 7), and the setting of w to zero when the RM-81000 sensor measures vertical wind speeds below its set threshold (in this case the threshold was at the lowest setting of 0.01 m s^{-1}, cf. between 40 and 50 s, Panel B, Fig. 7).

A 15-min averaging period was used for analyses of field data based on the ogives for stable, near neutral and slightly unstable conditions (Fig. 8). The overall results were the same using a 30-min averaging period (data not shown). There was large variability in the performance of each SAT among stability classes, wind and temperature statistics (Table 2). Small values of σ_T^2 under near neutral atmospheres likely contributed towards more relative variability in σ_T^2 and $\overline{w'T'}$ among SATs (Table 2). Longer scalar mixing lengths relative to sonic path lengths (cf. Table 1) likely contributed towards some of the observed variability among SATs under stable conditions. Thus, assuming SATs perform more uniformly in unstable atmospheres some common patterns in behavior among SATs emerge. The non-rotated estimates from the CSAT-3 generally had higher

estimates of $\overline{T_s}$, σ_T^2, $\overline{w_s}$, σ_w^2, and $\overline{w'T'}$, and lower estimates of $\bar{u}$ and σ_u^2 among all other SATs. Applying the 2-D coordinate framework generally did not improve any of the comparisons, with the exception of σ_w^2, and $\overline{w'T'}$ from the a-probe. Two notable exceptions to this pattern were: (i) both estimates of the σ_w^2 from the DA-600 was 13–15% higher than that found by the CSAT-3, (ii) the σ_T^2 from the SAT-550 was 21% higher than estimates from the CSAT-3 in slightly stable conditions, and (iii) the variability and slope in non-rotated $\overline{w_s}$ from the RM-81000 were less than that found from all other SATs (Table 2). The offsets for σ_u^2 and in not-rotated σ_w^2 were small or non-significant among all SATs.

Here, we provide a guideline to interpreting the data collected from each SAT as they compare to the CSAT-3 performance as presented in Table 2 and Appendix C.

3.3.1. k-Probe

$\overline{T_s}$ compared well, but was systematically less (~2–4%) in comparison across stabilities. σ_T^2 compared similarly well (less a few percentages). The non-rotated $\overline{w_s}$ was lower than that measured by the CSAT-3 by 33–41% in unstable atmospheres, but its variance compared

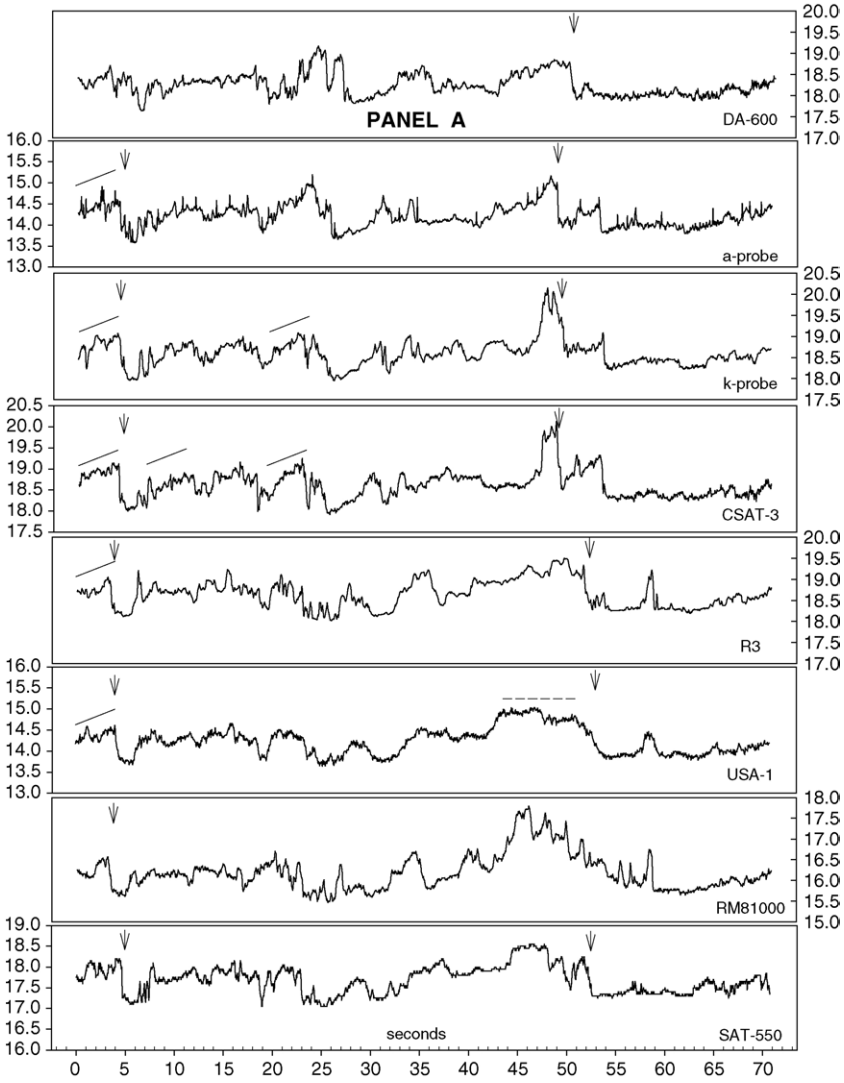

Fig. 7. A representative time series data of sonic temperature (Panel A) and vertical velocities (Panel B) from each SAT. Data were collected during the field experiment at September 28, 2004, 14:41:00 PST at 20 Hz, except for the SAT-550, which was collected at 50 Hz. The *y*-axes in Panel A all range 3 °C, all the *y*-axes in Panel B are ±0.6 m s^{-1} except for the RM-81000 data, which ranged −0.06 to 0.08 m s^{-1}. Winds were from 359° and mean horizontal wind speed was 1.37 m s^{-1} in a slightly unstable atmosphere.

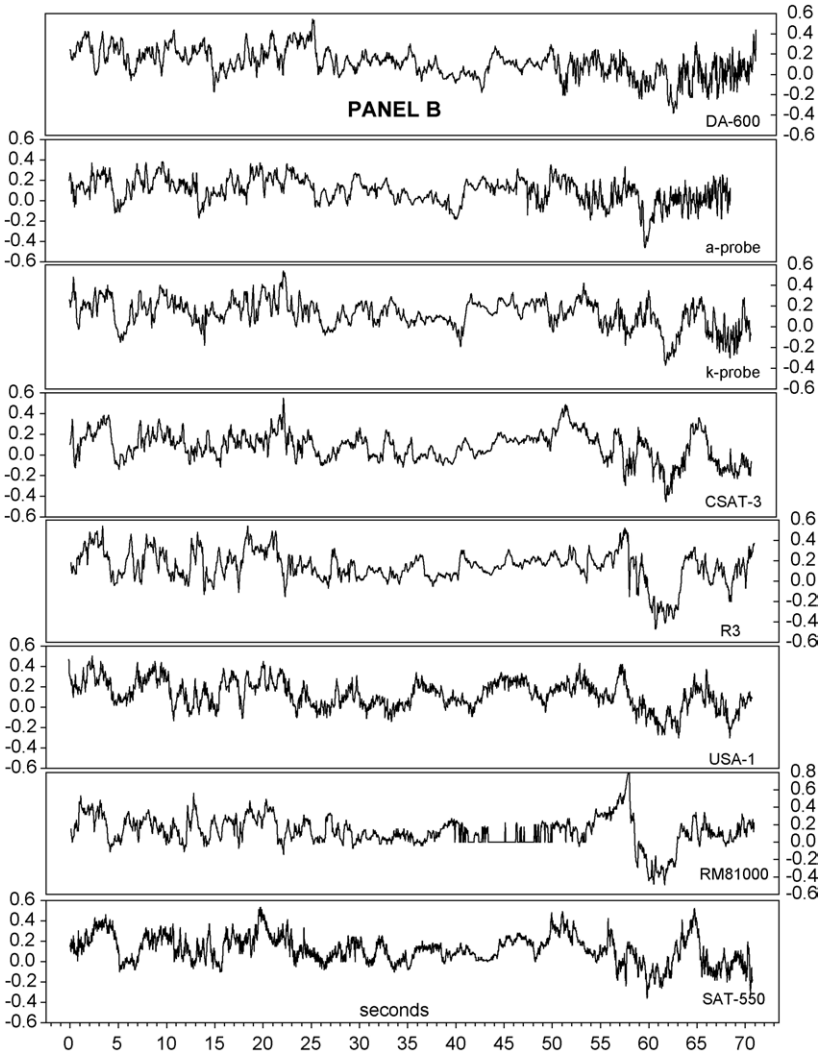

Fig. 7. (*Continued*).

very well. Applying the 2-D coordinate framework lowered the variance in vertical wind speed relative to the CSAT-3. Rotated $\bar{u}$ and σ_u^2 were both higher than the CSAT sensor. Non-rotated and rotated $\overline{w'T'}$ compared well for unstable atmospheres, and applying the coordinate framework improved the comparison of $\overline{w'T'}$ to within a few percent. Cospectral peaks shifted to higher frequencies with increasing stability, and a $-2/3$ slope in the inertial subrange was present for unstable, slightly unstable and near neutral atmospheres. 1:1 slope was observed in the lower frequencies under stable conditions which were balanced by $1{:}-1$ slopes in the higher frequencies, indicating that the k-probe was able to measure production (buoyancy forces) and dissipation (kinetic forces).

3.3.2. a-Probe

$\overline{T_s}$ also compared well, but was systematically less ($\sim$2–4%) in comparison across stabilities, but was only able to capture the same σ_T^2 under unstable atmospheres. In all other stabilities, the σ_T^2 did not compare well. Conversely, non-rotated $\overline{w_s}$ compared well in slightly unstable and stable atmospheres, but was $\sim$26% lower than estimates measured by this CSAT-3 sensor in unstable conditions. The σ_T^2 improved from $\sim$50% of the measured variance by the CSAT to within a few percent after the 2-D coordinate framework was applied. The a-probe estimates of non-rotated $\overline{w'T'}$, rotated $\bar{u}$, σ_u^2, and $\overline{w'T'}$ were higher than that from the CSAT sensor following the same trends estimated by the k-probe. The overall cospectral shape and peak did not change among stabilities.

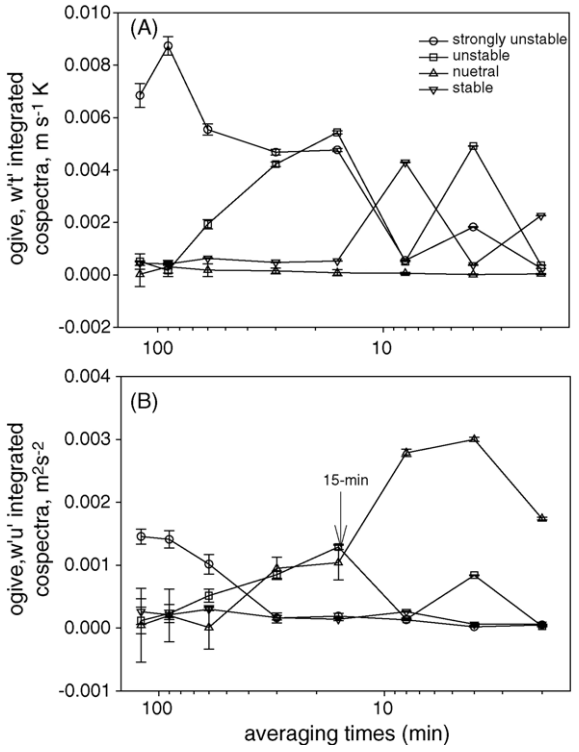

Fig. 8. The relationship between different averaging periods and integrated cospectra (ogive) for (A) $w'T'$ and (B) $w'u'$ from CSAT-3 data collected September 28–October 8, 2004, from the Hyslop research site, Corvallis, OR. Cospectra were integrated between frequencies 0.1 and 20 Hz. Vertical wind velocities were rotated into mean stream flow (i.e., 2-D rotation). Error bars are ±1 S.D. Strongly unstable, unstable, neutral, and stable conditions were determined by $\varsigma < -1$, $-1 < \varsigma < -0.0625$, $-0.0625 < \varsigma < -0.02$, and >0.02, respectively. x-Axis is log scale.

3.3.3. DA-600

$\overline{T_s}$ was lower by 7–16% in unstable atmospheres than that estimated by the CSAT-3 sensor, and was ∼16% higher in near neutral conditions. σ_T^2 followed the same trend as that observed for $\overline{T_s}$. Non-rotated $\overline{w_s}$ was the same in unstable atmospheres, but higher than that found by the CSAT-3 in slightly stable and near neutral conditions. σ_w^2 estimates, however, were consistently higher whether the coordinate rotation was applied or not, and ranged 13–144% higher. The σ_u^2 were also consistently higher among all stabilities than those found by the CSAT sensor. Non-rotated $\overline{w'T'}$ was identical, in comparison, under unstable conditions, but was only 23% of the CSAT estimates in near neutral atmospheres. Applying the 2-D rotation improved $\overline{w'T'}$ estimates in near neutral conditions and increased $\overline{w'T'}$ estimates 5–8% compared to the CSAT sensor. Shifts in the copsectral peaks with increasing stability were observed and the DA-600 demonstrated similar ability to measure both the buoyancy and kinetic terms in the stable atmosphere as that of the k-probe.

3.3.4. SAT-550

$\overline{T_s}$ and σ_T^2 slopes were close to 1 except under slightly unstable conditions when $\overline{T_s}$ measured 18% lower and σ_T^2 estimates where 21% higher than those measured by the CSAT-3. There were limited field data collected with this sensor. The non-rotated $\overline{w_s}$ was lower by 10–20%, non-rotated σ_w^2 was 1–5% lower in unstable atmospheres than that measured by the CSAT-3. Once the coordinate framework was applied, the variance of vertical wind speed was in less agreement, but improved the agreement in $\overline{w'T'}$ between the two sensors, from −29 to 6% in slightly unstable conditions. Rotated $\bar{u}$ and σ_u^2 were both higher than the CSAT sensor.

3.3.5. R3

$\overline{T_s}$ compared well, but was systematically less (∼2–5%) in comparison across stabilities. σ_T^2 compared similarly well (less a few percentages). The non-rotated $\overline{w_s}$ was ∼35% lower than that estimated by the CSAT-3. Non-rotated σ_w^2 compared well, but less agreement in σ_w^2 between the two sensors after rotation was applied (particularly in unstable atmospheres). A similar trend was observed in comparing $\overline{w'T'}$ before and after the coordinate framework was applied. Rotated $\bar{u}$ was ∼8% higher under near neutral and unstable atmospheres. Cospectral peaks shifted to higher frequencies with increasing stability, and a −2/3 slope in the inertial subrange was present for unstable, slightly unstable and near neutral atmospheres. But the R3's ability to estimate lower frequency turbulence (buoyancy terms) under stable conditions was not as apparent as with some of the other sensors.

3.3.6. USA-1

$\overline{T_s}$ was consistently lower by ∼15% among all stabilities. Similarly, σ_T^2 compared lower, ranging 7–23% less than CSAT-3 estimates. The non-rotated $\overline{w_s}$ was ∼58 and 36% lower in unstable atmospheres. Similarly, non-rotated σ_w^2 compared was systematically lower by 10–21%. Applying a coordinate rotation did not improve the σ_w^2 estimate. Rotated $\bar{u}$ and σ_u^2 were both higher than the CSAT sensor (with the exception for σ_u^2 under near neutral conditions). $\overline{w'T'}$ compared lower before and after the coordinate framework was applied, by 15–19% among all stabilities. Cospectral peaks shifted to higher frequencies between unstable and stable atmospheres, and a −2/3 slope in the inertial subrange was present for unstable, slightly unstable and near neutral atmospheres. Though the USA-1 demon-

Table 2
Field comparison between non-rotated and 2-D rotated wind statistics from the CSAT-3 to the other model SATs among stability classes. Stability was defined by unstable ($\varsigma < -1$), slightly unstable ($-1.0 < \varsigma < -0.0625$), near neutral ($-0.0625 < \varsigma < 0.02$), and stable ($\varsigma > 0.02$). Data were collected from September 28 to October 8, 2004, from Oregon State University Hyslop Research site. Least squares first-order regression analyses were made on 15-min averages, data presented as slope, *y*-intercept, R^2. Data were also removed when conditions of non-stationary were met using (3) 5-min periods following Foken and Wichura (1996). Approximately (524) 15-min averages from each model SAT were used for these comparisons

	Sonic model	Unstable	Slightly unstable	Near neutral	Stable
$\overline{T_s}$	k-Probe	0.97, 0.35, 0.91	0.98, 0.10, 0.92	0.96, 0.85, 1.00	0.96, 0.65, 0.97
	a-Probe	0.94, −3.20, 0.99	0.97, −3.96, 0.99	0.97, −3.86, 1.00	0.91, −2.52, 1.00
	DA-600	0.84, 3.19, 0.84	0.93, 1.03, 0.95	1.16, −4.01, 0.97	0.96, 0.19, 0.92
	SAT-550	1.00, −1.04, 1.00	0.82, 1.19, 0.81	0.99, −0.96, 1.00	1.00, −1.01, 1.00
	R3	0.95, 0.92, 0.98	0.99, 0.53, 0.98	0.96, 1.69, 1.00	0.98, 1.43, 1.00
	USA-1	0.84, −1.59, 0.99	0.87, −2.09, 0.99	0.85, −1.54, 1.00	0.85, −1.64, 1.00
	RM-81000	0.99, −2.14, 0.98	1.02, −2.79, 0.99	1.00, −2.57, 1.00	0.94, −1.55, 1.00
σ_T^2	k-Probe	0.98, ns, 0.89	0.93, ns, 0.88	0.96, ns, 0.98	0.99, ns, 0.99
	a-Probe	0.99, −0.21, 0.93	0.76, −0.11, 0.82	0.28, −0.02, 0.94	0.75, −0.1, 0.92
	DA-600	0.85, 0.15, 0.13	0.95, −0.01, 0.91	1.25, −0.02, 0.90	1.17, 0.05, 0.18
	SAT-550	1.00, ns, 1.00	1.21, ns, 0.94	1.02, ns, 0.99	1.00, ns, 1.00
	R3	0.95, ns, 0.96	0.98, −0.01, 0.97	0.68, 0.03, 0.92	0.95, ns, 0.98
	USA-1	0.90, ns, 0.98	0.93, ns, 0.98	0.77, 0.02, 0.98	0.94, ns, 0.99
	RM-81000	0.92, 0.04, 0.88	0.95, ns, 0.91	0.50, 0.09, 0.44	0.96, 0.01, 0.94
Non-rotated $\bar{w}$	k-Probe	0.59, 0.03, 0.74	0.66, 0.02, 0.72	0.95, ns, 0.72	0.61, 0.2, 0.80
	a-Probe	0.74, 0.04, 0.72	0.97, 0.03, 0.54	1.35, ns, 0.58	0.98, 0.03, 0.74
	DA-600	1.00, 0.06, 0.67	1.19, 0.04, 0.72	1.23, 0.03, 0.46	1.09, 0.4, 0.75
	SAT-550	0.90, 0.03, 0.91	0.82, 0.03, 0.78	na	0.80, 0.03, 0.69
	R3	0.65, 0.03, 0.43	0.64, 0.02, 0.29	0.71, 0.02, 0.34	1.08, 0.03, 0.63
	USA-1	0.42, 0.05, 0.15	0.64, 0.04, 0.18	0.87, 0.05, 0.28	1.42, 0.07, 0.50
	RM-81000	0.35, 0.01, 0.13	0.32, ns, 0.06	0.58, −0.04, 0.18	0.59, 0.01, 0.27
Non-rotated σ_w^2	k-Probe	1.00, −0.02, 0.94	0.99, −0.02, 0.95	0.92, −0.01, 0.96	0.94, −0.02, 0.99
	a-Probe	0.40, −0.04, 0.93	0.43, −0.04, 0.94	0.59, −0.09, 0.69	0.62, −0.06, 0.83
	DA-600	1.13, ns, 0.95	1.15, ns, 0.93	1.23, −0.03, 0.91	1.34, −0.02, 0.92
	SAT-550	0.99, ns, 1.00	0.95, ns, 0.99	0.90, ns, 1.00	0.91, ns, 1.00
	R3	1.00, ns, 0.99	0.98, ns, 0.98	0.89, 0.02, 0.95	0.93, ns, 0.98
	USA-1	0.90, 0.01, 0.99	0.87, 0.01, 0.98	0.79, 0.02, 0.98	0.81, 0.02, 0.98
	RM-81000	1.04, −0.01, 0.94	1.01, −0.01, 0.96	0.80, 0.03, 0.80	0.95, ns, 0.93
Non-rotated $\overline{wT}$	k-Probe	0.93, ns, 0.95	0.93, ns, 0.97	0.73, ns, 0.94	0.86, ns, 0.78
	a-Probe	0.93, ns, 0.96	0.91, ns, 0.96	0.39, ns, 0.43	1.18, ns, 0.63
	DA-600	1.00, ns, 0.95	1.00, ns, 0.95	0.23, ns, 0.09	1.33, ns, 0.28
	SAT-550	0.91, ns, 0.98	0.71, ns, 0.89	1.20, ns, 0.99	0.79, ns, 0.53
	R3	0.95, ns, 0.96	1.00, ns, 0.97	1.17, ns, 0.93	0.84, ns, 0.52
	USA-1	0.85, ns, 0.95	0.83, ns, 0.94	0.86, ns, 0.88	0.67, ns, 0.37
	RM-81000	0.92, ns, 0.93	1.00, ns, 0.94	0.79, ns, 0.87	0.62, ns, 0.35
Rotated $\bar{w}$	k-Probe	na	−0.24, ns, 0.09	−0.34, ns, 0.27	na
	a-Probe	na	na	na	na
	DA-600	na	na	na	na
	SAT-550	na	na	na	na
	R3	na	na	0.30, ns, 0.20	na
	USA-1	na	na	na	na
	RM-81000	na	na	na	na
Rotated σ_w^2	k-Probe	0.88, ns, 0.98	0.91, ns, 0.97	0.92, ns, 0.99	0.83, ns, 0.99
	a-Probe	1.01, ns, 0.97	0.94, ns, 0.92	0.96, ns, 0.98	1.60, −0.03, 0.93
	DA-600	1.43, ns, 0.85	1.46, −0.01, 0.84	1.20, ns, 0.99	2.44, −0.01, 0.94
	SAT-550	na	0.89, ns, 0.99	na	0.85, ns, 1.00
	R3	1.05, ns, 0.71	0.93, ns, 0.95	1.00, ns, 1.00	0.85, ns, 0.99
	USA-1	0.87, ns, 0.88	0.84, ns, 0.95	0.81, ns, 1.00	0.74, ns, 0.96
	RM-81000	0.92, ns, 0.60	0.91, ns, 0.93	1.06, ns, 0.96	0.84, ns, 0.75

Table 2 (*Continued*)

	Sonic model	Unstable	Slightly unstable	Near neutral	Stable
Rotated $\bar{u}$	k-Probe	1.07, −0.09, 0.87	1.07, −0.08, 0.93	1.05, −0.12, 0.99	1.45, −0.25, 0.90
	a-Probe	1.02, −0.04, 0.92	1.02, −0.03, 0.96	0.98, 0.04, 0.99	1.49, −0.62, 0.90
	DA-600	0.95, −0.12, 0.91	0.91, −0.09, 0.95	0.88, −0.11, 0.99	1.07, −0.14, 0.92
	SAT-550	na	1.13, −0.16, 0.96	na	1.11, −0.11, 0.98
	R3	1.08, −0.04, 0.86	1.09, −0.04, 0.98	1.08, −0.09, 1.00	1.45, −0.21, 0.90
	USA-1	1.11, −0.08, 0.87	1.12, −0.08, 0.92	1.10, −0.10, 1.00	1.51, −0.23, 0.90
	RM-81000	1.06, −0.07, 0.88	1.06, −0.04, 0.84	1.16, −0.14, 0.97	1.36, −0.19, 0.82
σ_u^2	k-Probe	1.12, 0.01, 0.84	1.04, 0.02, 0.87	0.95, 0.01, 0.99	1.30, ns, 0.87
	a-Probe	1.03, 0.02, 0.91	0.89, 0.06, 0.84	0.99, 0.02, 0.99	1.26, −0.04, 0.98
	DA-600	1.30, −0.01, 0.59	1.05, 0.09, 0.65	1.33, 0.05, 0.53	1.83, −0.02, 0.78
	SAT-550	na	1.69, −0.06, 0.92	na	1.02, ns, 1.00
	R3	1.16, 0.01, 0.85	0.99, 0.03, 0.87	0.91, 0.02, 0.96	1.14, 0.01, 0.82
	USA-1	1.25, 0.01, 0.84	1.06, 0.03, 0.88,	0.96, 0.03, 0.97	1.21, 0.01, 0.83
	RM-81000	1.16, 0.01, 0.81	0.91, 0.4, 0.79	1.16, −0.02, 0.83	1.03, 0.02, 0.68
Rotated $\overline{wT}$	k-Probe	0.93, ns, 0.98	0.96, ns, 0.99	0.95, ns, 0.99	0.71, ns, 0.53
	a-Probe	0.94, ns, 0.95	0.96, ns, 0.96	0.90, ns, 0.95	1.39, ns, 0.87
	DA-600	1.05, ns, 0.95	1.08, ns, 0.95	1.06, ns, 0.84	1.16, ns, 0.34
	SAT-550	na	1.06, ns, 0.96	na	na
	R3	0.88, ns, 0.83	1.00, ns, 0.97	1.00, ns, 0.90	0.88, ns, 0.68
	USA-1	0.81, ns, 0.92	0.89, ns, 0.96	0.84, ns, 0.93	1.05, ns, 0.41
	RM-81000	0.86, ns, 0.90	0.94, ns, 0.94	1.15, ns, 0.83	0.27, ns, 0.07

strated a spectral peak in near neutral atmospheres at lower frequencies more akin to that found in unstable conditions. Moreover, aliasing effects can be clearly observed under stable conditions that extend into the inertial subrange.

3.3.7. RM-81000

$\overline{T_s}$ compared well, with slope close to 1, but with a significant negative offset ∼2.00 °C among unstable and near neutral stabilities. σ_T^2 also compared reasonably well in unstable atmospheres. The non-rotated $\overline{w_s}$ was uniformly lower among all stabilities. Conversely, non-rotated σ_w^2 compared well with slopes ranging 1.04–1.01 in unstable atmospheres. After rotating the coordinates, σ_w^2 compared well, but with slightly lower slopes, ranging 0.92–0.91 in unstable conditions. Both rotated $\bar{u}$ and σ_u^2 compared higher than estimates found with the CSAT sensor. Non-rotated $\overline{w'T'}$ compared well in unstable conditions, but once the 2-D rotation was applied, lowered the comparison by 6%. Under stable conditions, however, $\overline{w'T'}$ was 38 and 73% lower with non-rotated and rotated framework, respectively, even though the variances of $\overline{w_s}$ and $\overline{T_s}$ compared reasonably well. Overall cospectral response was similar to those found by the CSAT sensor.

3.4. Modeled buoyancy flux

The percent difference between $\overline{w'T'_{mod}}$ and $\overline{w'T'_{prt}}$ for each 15-min averaging period ranged −23.1 to +16.1%

Table 3
The percent difference between $\overline{w'T'_{prt}}$ and $\overline{w'T'_{mod}}$, buoyancy flux among SATs. The 20 Hz time series from the CSAT-3 collected at Hyslop research site was back-corrected to fit the response to $\overline{T_a}$, and $\overline{w'T'_{prt}}$ estimated. Then, the specific response function of $\overline{T_s}$ to $\overline{T_a}$ from each model SAT was applied to the same time series ($\overline{w'T'_{mod}}$). The potential error in the buoyancy flux was determined by subtracting $\overline{w'T'_{prt}}$ and $\overline{w'T'_{mod}}$. Stability was defined by unstable ($\varsigma < -1$), slightly unstable ($-1.0 < \varsigma < -0.0625$), near neutral ($-0.0625 < \varsigma < 0.02$), and stable ($\varsigma > 0.02$). Data presented as mean, minimum, and maximum percent difference between $\overline{w'T'_{prt}}$ and $\overline{w'T'_{mod}}$

SAT model	Unstable	Slightly unstable	Near neutral	Stable
CSAT-3	1.8, −8.9, 9.3	2.0, −9.8, 10.3	4.8, −0.2, 9.7	1.1, −10.5, 11.0
a-Probe	0.4, −6.5, 7.4	0.1, −5.2, 5.5	1.9, −1.5, 5.2	−0.42, −5.1, 5.0
k-Probe	0.4, −9.2, 10.6	0.2, −7.2, 7.8	−2.3, −2.7, 7.2	−0.7, −7.1, 7.0
R3	2.0, −11.9, 12.5	2.5, −13.4, 14.1	4.9, −3.3, 13.1	1.6, −14.4, 15.4
SAT-550	2.7, −11.9, 12.3	2.7, −12.8, 13.3	7.8, 2.9, 12.7	−1.3, −13.5, 14.0
DA-600	0.7, −19.3, 16.1	1.7, −12.7, 13.0	0.1, −11.4, 11.5	1.9, −13.3, 14.7
USA-1	−0.4, −7.4, 6.5	−0.1, −5.5, 5.2	−1.9, −5.2, 1.5	0.5, −5.0, 5.1
RM-81000	1.0, −23.1, 6.2	1.4, −6.6, 9.5	3.2, −0.2, 6.5	−0.7, −13.6, 20.4

(Table 3). The largest mean percent difference among all the averaging periods ($n = 940$) was <8%, and occurred in near neutral atmosphere with the exception of the DA-600, which the largest mean difference was under stable conditions. Differences in H in slightly unstable atmospheres (as estimated between $\overline{w'T'_{\mathrm{mod}}}$ and $\overline{w'T'_{\mathrm{prt}}}$, Eq. (A.4), Appendix A) ranged from −19 to +14% for any 15-min averaging period, and ranged from −1 to +8% when averaged over ∼940 15-min periods.

4. Discussion

4.1. Acoustically isolated chamber

The offset and functional relationship of $\overline{T_{\mathrm{s}}}$ to $\overline{T_{\mathrm{a}}}$ differed among SAT models and it is likely different for each individual SAT. Researchers should not use $\overline{T_{\mathrm{s}}}$ as an estimate of virtual temperature unless the specific response to $\overline{T_{\mathrm{a}}}$ is empirically quantified and calibrated to a standard (NIST traceable) temperature sensor for each SAT used. The estimation of $\overline{w'T'}$ is likely not affected if the relationship of $\overline{T_{\mathrm{s}}}$ to $\overline{T_{\mathrm{a}}}$ is linear. But great care should be taken if $\overline{T_{\mathrm{s}}}$ is used for other calculations, for example, the determination of the molar volume of air, heat capacity of air, and WPL unit conversion for other scalar fluxes (cf. Massman, 2004; Luening, 2004). If the response of $\overline{T_{\mathrm{s}}}$ to $\overline{T_{\mathrm{a}}}$ is non-linear for all or any part of the range of ambient temperatures, however, the accurate estimation of $\overline{T_{\mathrm{s}}}$, and hence, $\overline{w'T'}$ is in question, for example, the Gill R3 at $\overline{T_{\mathrm{s}}} < 5\,^{\circ}\mathrm{C}$ (Fig. 4). $\overline{T_{\mathrm{s}}}$ from other models of Gill sonics (i.e., R2, windmaster pro) may exhibit a curvilinear response to $\overline{T_{\mathrm{a}}}$ starting at ∼18 °C (C. Stock and H. Loescher, personal communication). Both ATI sensors also behaved non-linearly to $\overline{T_{\mathrm{a}}}$ but only when operated outside its calibrated range, so we strongly recommend assuring that all data collected with the ATI SATs are within its calibrated range, i.e., ±10 °C of its calibrated temperature. We also caution that the rather good results presented here are over a modest temperature range should not be interpreted to imply linear behavior of $\overline{T_{\mathrm{s}}}$ outside this range. Hence, for these reasons and those stated above, researchers who use these SATs should determine the relationship between $\overline{T_{\mathrm{s}}}$ and $\overline{T_{\mathrm{a}}}$, and correct if necessary for any non-linearity in SAT estimates. Alternatively, researchers may wish to have this relationship quantified by the manufacturer.

The significant relationships of $\overline{w_{\mathrm{s}}}$ and σ_w^2 among chamber temperatures had little affect on vertical and horizontal velocities, meaning that measured wind speeds in the ambient environment can be valid when there is an offset in $\overline{T_{\mathrm{s}}}$ from $\overline{T_{\mathrm{a}}}$.

4.2. Wind tunnel

SATs were placed in the wind tunnel so that they would experience the greatest amount of flow distortion in $\overline{w_{\mathrm{s}}}$ within the manufacturer specifications (cf. Table 1) and within the range of observed $\bar{w}$ from typical field applications. All SATs estimates of $\bar{w}$ did not behave linearly with the hot-film estimates (Figs. 5 and 6). All post-style SATs overestimated (updraft) $\overline{w_{\mathrm{s}}}$ at flows $<0.1\ \mathrm{m\ s^{-1}}$ with the SAT-550 showing the greatest difference when stanchions were not in the mean flow path (Figs. 5 and 6). These results suggest that inflections in flow off the cylindrical base reach the measured sonic volume. Conversely, the a-, k-probe and CSAT-3 sensors underestimated $\bar{w}$ at $\sim 0.28\ \mathrm{m\ s^{-1}}$, also suggesting that flow distortions from the housing reach the sonic volume (Fig. 6). We discount any significant error due to the calibration of the hot-film sensor or flow distortions from the hot-film sensor from its relative position inside the wind tunnel because the calibrations were verified by the calibration system provided by the manufacturer, and the position was in the mean flow regime of the tunnel away from any immediate influence from other bodies.

We have similar concerns about the usage of $\overline{w_{\mathrm{s}}}$ as we have about $\overline{T_{\mathrm{s}}}$ because of the non-uniform behavior in $\overline{w_{\mathrm{s}}}$ of SATs to that of $\overline{w_{\mathrm{hf}}}$. Accurate estimates of $\overline{w_{\mathrm{s}}}$ are needed in advection studies (cf. Lee, 1998), planar rotation schemes (Wilczak et al., 2001) and also for the WPL unit conversion. The lack of agreement in $\overline{w_{\mathrm{s}}}$ among sensors and the apparent non-linearity in $\overline{w_{\mathrm{s}}}$ at low flows (similar to those observed in field applications) call into question our ability to accurately estimate the advection terms (cf. Lee, 1998; Paw et al., 2000) and the WPL conversion. Researchers using more than one SAT should calibrate $\overline{w_{\mathrm{s}}}$ from each sensor to a uniform standard (or to the response of a single SAT) to minimize the systematic error in $\overline{w_{\mathrm{s}}}$ among sensors.

4.3. Field experiment

In the field study, if the turbulent fluctuations of sonic temperature (T'_{s}) in the ambient environment exhibited linear behavior to T'_{a}, we would expect σ_T^2 would compare similarly among stability classes and SATs. With the exception of the ATI k-probe, σ_T^2 from each model SAT compared poorly in, at least, one stability class, ranging between −50 and +21% of CSAT-3 σ_T^2 (Table 2) for any particular 15-min averaging period. Because we adopted the CSAT-3 as a standard, σ_T^2 from all sonics did not behave similarly and did not follow any systematic trend within or among averaging

periods. These results suggest that the ability of each model SAT to determine $\overline{T_s}$ and T_s' differs across a range of temperatures and stabilities. Some errors may exist due to random effects and sensor separation, but we would expect them to account for only a few percent in the comparison (Loescher et al., submitted for publication; Kristensen et al., 1997; Moncrieff et al., 1996). Errors may also exist due to heterogeneity in the flows over the field not accounted for by the stationarity test, but these effects were discounted because of the lack of extreme surface heating and the relatively uniform environmental conditions during the test.

An increase in spectral energy can be observed in $\overline{T_s}$ and $\overline{w_s}$ spectra from some SATs, seen as a positive slope in high frequencies (Appendix B), and were most apparent across all stabilities in the USA-1 data. The increase in spectral energy became more apparent as spectral peaks shift toward the lower frequencies under near neutral and stable atmospheres. The source of which was likely due to more random behavior in the natural turbulent environment, higher noise-to-signal ratio in the model SAT, aliased data outside the Nyquist cutoff frequency, effects of block averaging, or some combination thereof (cf. Kaimal and Finnigan, 1994). This additional spectral energy may also explain some of the poor agreement in $\overline{T_s}$ and $\overline{w_s}$ statistics under near neutral and stable atmospheres (Table 2), but it did not contribute towards $\overline{w'T'}$ with the exception of data from the USA-1. The observed spectra from R3 consistently appeared as the idealized spectra discussed in Kaimal and Finnigan (1994), and a notable improvement from that found in Wieser et al. (2001).

Uncertainties in $\overline{T_s}$ may be the result of gain errors from environmentally induced changes in the path-length geometry during our field experiment (cf. Eq. (3)). The fractional error in $\overline{T_s}$ is twice the fractional change in path distance. We did not empirically measure the changes in path length, though the uncertainties associated with errors in gain are likely to be small, for example, a 0.33% change in sonic path length (or 360 μm for the CSAT-3) represents a gain error of 0.67% in $\overline{T_s}$ and correspondingly, a 0.67% error in $\overline{w'T'}$. Changes in the SAT geometry due to changes in temperature may explain the observed linear departure from a 1:1 line observed in SAT-550 and USA-1 sensors (Fig. 4). Moreover, σ_T^2 estimates within the acoustically isolated chamber did not change significantly across the range of tested temperatures also suggesting that the effects of heating or cooling of physical geometry of each SAT would contribute little error in $\overline{w'T'}$ estimates.

Errors in the measurement of $\overline{w_s}$ and σ_w^2, however, likely contribute greater uncertainties to the estimation of scalar fluxes. Even though Gash and Dolman (2003) used vertical velocities $\geq$2 m s^{-1}, data from this study supports their findings that SATs have difficulty in measuring winds with large angles of attack through the overestimation of $\overline{w_s}$ in the wind tunnel by post-style SATs (at ∼0.1 m s^{-1}, Fig. 5), and the underestimation of $\overline{w_s}$ by the CSAT-3, a- and k-probes (at ∼0.28 m s^{-1}, Fig. 6). The attack angles used here were within the manufacturer's specifications, while Gash and Dolman (2003) used attach angles outside the specification of the R2 and R3 SATs. But there were no large attack angles in the field data, and $\overline{w_s}$ and σ_w^2 still compared poorly among some SATs. We could not determine if the flow distortions that caused errors in $\overline{w_s}$ also affect σ_w^2, though we did find that changes in $\overline{T_s}$ can affect $\overline{w_s}$ and σ_w^2 from some SATs. Another systematic source of error among $\overline{w_s}$ and σ_w^2 measurements may derive from different methods used to determine the x-, y-, and z-vectors from each model SAT. It is possible that each model SAT partitioned the total turbulent structure into slightly different vectors as evidenced by anomalous features in the time series (Panel B, Fig. 7), and by the observation that the CSAT-3 estimates of $\overline{w_s}$ were generally higher and estimates of $\bar{u}$ were lower than that estimated by most all other SATs.

In this field comparison, the wind and temperature statistics were averaged over 15-min among all SATs. Hence, the temporal scale was identical for all SATs, and we assume all SATs captured all the motions that contributed to the covariance of $\overline{w'T'}$ in unstable atmospheres (Table 2). The non-uniform shifts in the $\overline{w'T'}$ cospectral peaks and the non-uniform −2/3 relationship in the inertial subrange among SATs suggest the inability of each SAT to uniformly measure the scale of turbulence that contributed to the flux either due to the physical design of the SAT or the sensor separation. The agreement in $\overline{w'T'}$ was generally better in unstable than stable atmospheres, which suggests the notion that each SAT measures the scale of turbulence differently. If fewer assumptions are likely violated under slightly unstable conditions, then uncertainty in H among sensors (due to their different responses to $\overline{T_a}$) ranged −19 to +14% for any specific 15-min averaging period, and range −1 to +8% as an overall average, and may actually be larger if differences in the response in $\overline{w_s}$ were taken into account. This result was also true using a 30-min averaging period, suggesting that $\overline{w'T'}$ and H compares reasonably well among sensors across longer time intervals, i.e., >7 d, but cannot explain all the

variability in shorter time integrals, i.e., averaging period-to-averaging period.

There is not only uncertainty among SATs, but it is also very likely that SAT measurements from the same manufacturer differ. For all the sources of uncertainty outlined above, precise SAT measurements are relative to the specific instrument used. Because systematic error temporally scales with the estimates, this study also provides a basis to estimate uncertainties associated with SATs and how these uncertainties may contribute to other research that use multiple SATs for comparisons across sites, or those that scale flux estimates temporally and spatially using different model SATs.

Acknowledgements

This research was supported by the Office of Science (BER), U.S. Department of Energy, Grant Numbers DE FG02-03ER63624 as part of NACP. Authors wish to thank R. Vogt, H.-J. Kirtzel, D. Poinsett, and T. Pypker for careful and thoughtful internal reviews, M. Byrkit for assistance, L. Mahrt and S.R. Radosevich for use of equipment, the OSU College of Agriculture Sciences for generously providing field access, and to D. Fitzjarrald and to other anonymous reviewers for their careful and thoughtful comments.

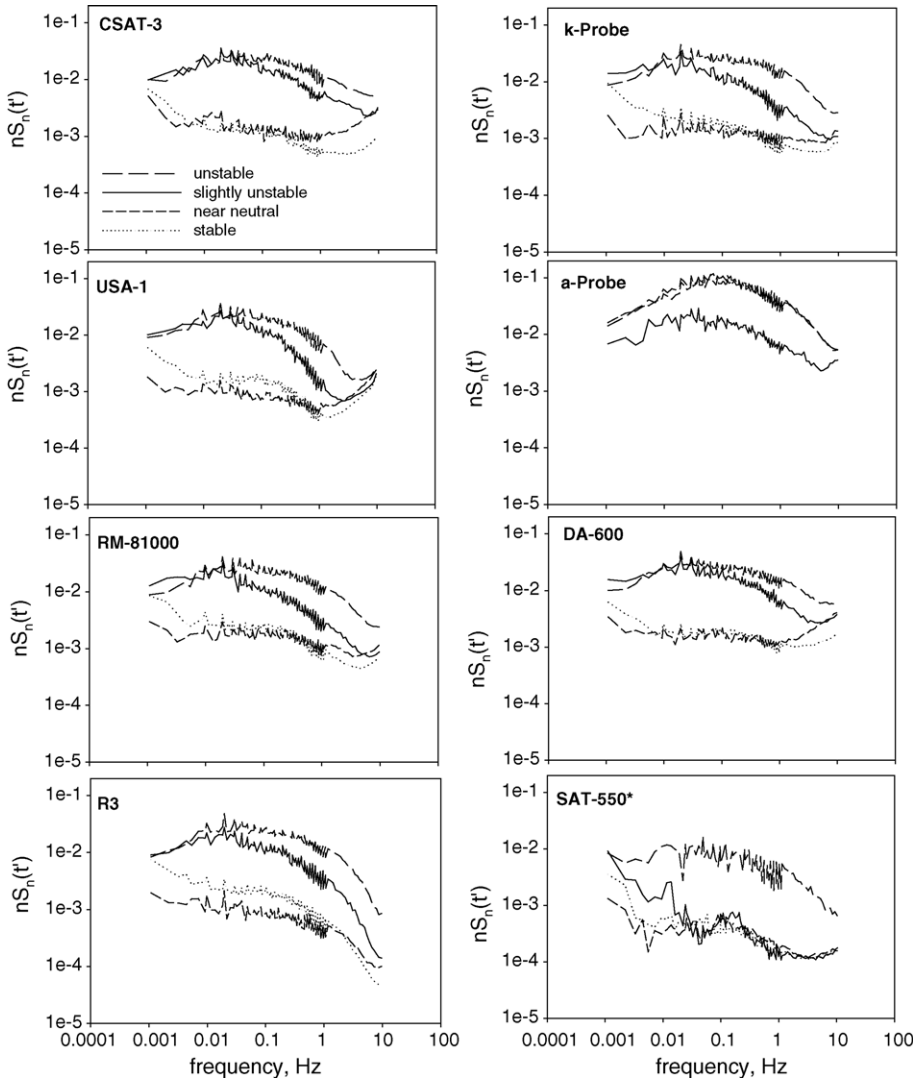

Fig. B.1.

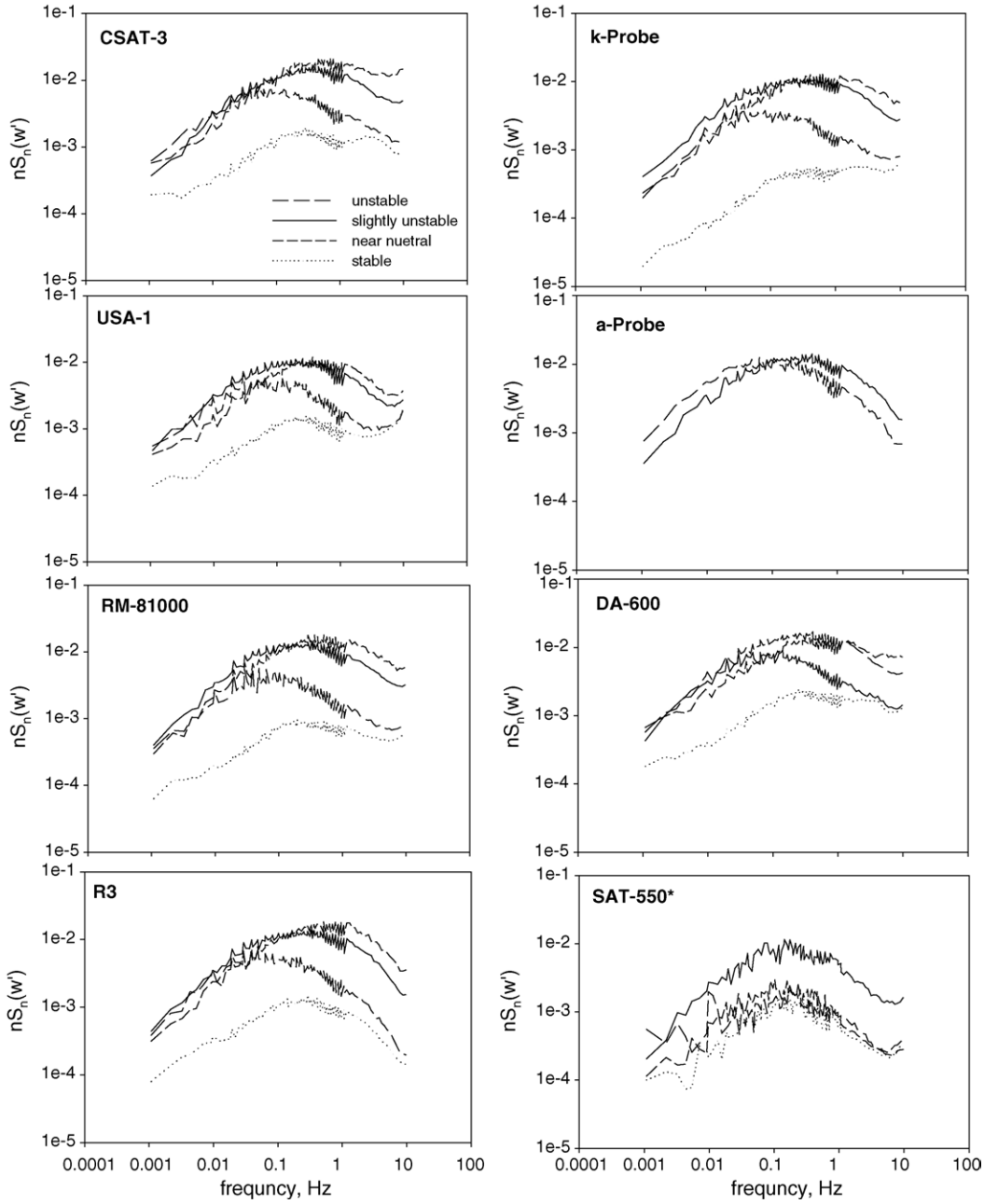

Fig. B.2.

Appendix A

Other calculations used in this study that are the subject of discussion in numerous reviews (cf. Loescher et al., submitted for publication; Baldocchi, 2003).

Vapor pressure of water (e) was calculated by,

$$e = e_s \frac{\mathrm{Rh}}{100} \tag{A.1}$$

where e_s is the saturation vapor pressure of water (Pa) at a known temperature, and Rh is the relative humidity, and in our case, checked with a sling psychrometer, and,

$$e_s = (1.0007 + 3.46 \times 10^{-8} P_a) \times \left[611.21 \exp \frac{17.502 \bar{T}}{240.97 + \bar{T}}\right] \tag{A.2}$$

after Buck (1981).

The covariance of $\overline{w'T'}$ was estimated by how the turbulent fluctuations of w_s and T_s co-vary, such that,

$$\overline{w'T'} \cong \overline{w'_s T'_s} = (w_s - \overline{w_s})(T_s - \overline{T_s}) \quad \text{(A.3)}$$

where $\overline{w'T'}$ is the covariance of turbulent fluctuations (noted by the prime) of the measured vertical wind speed, w_s (m s^{-1}) and T_s (°C), n is the sample size. The overbar indicates time-averaged quantities (in this study a 15-min averaging period was used, see Section 2) and the turbulent fluctuations are determined by the difference between measured and mean quantities).

Sensible heat flux was estimated by,

$$H = \left(\frac{M_a C_p P_a}{R T_s}\right)\overline{w'_s T'_s} \quad \text{(A.4)}$$

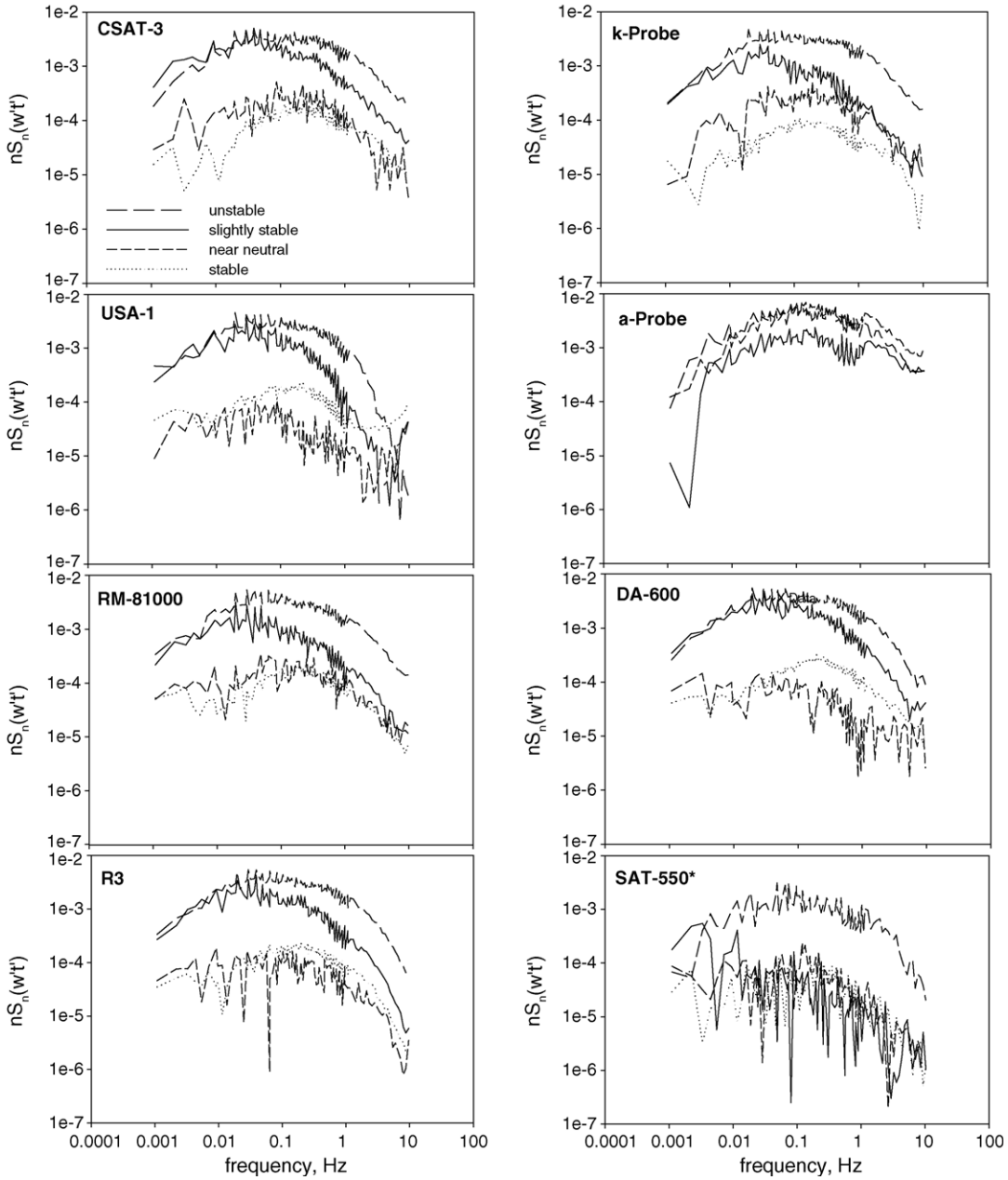

Fig. B.3.

noting that all SATs used here perform the crosswind correction internally before they report the speed of sound or sonic temperature.

Monin–Obukov similarity was used to determine the stability parameter,

$$\varsigma = -\frac{z}{L} \tag{A.5}$$

where z is the measurement height (2.75 m) and L is the ratio of convective to mechanical turbulent production,

$$L = \frac{u^{*3}\rho_a C_p T_s}{kgH} \tag{A.6}$$

where u^* is defined as friction velocity (m s^{-1}), ρ_a the density of air (g m^{-3}), k the von Kármán constant (0.41), and g is the acceleration due to gravity (m s^{-2}).

Appendix B

Spectra of $\overline{w_s}$ and $\overline{T_s}$, and cospectra of $\overline{w'T'}$ were ensembled by normalizing the spectra density with the variance, spectra data size of 2048 bytes, 100 output bins, and a hamming widow was used for each 15-min averaging period. Spectra were removed when: (i) wind directions were ±45° outside from the SAT orientation, (ii) precipitation occurred, and (iii) stationarity was >25%, then sorted and averaged by stability class (see Figs. B.1–B.3).

Appendix C

Mean vertical wind velocities from the Metek USA-1 SAT compared to hot-film measurements in the wind tunnel. Sonics were placed inside the wind tunnel 25° within the manufacturer's acceptance angles for the vertical component, i.e., $^{\circ}\theta_B = 20^{\circ}$ (see Fig. C.1).

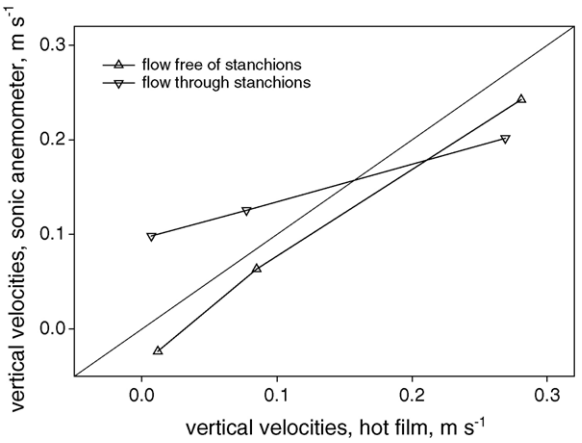

Fig. C.1.

References

Allan, D.W., 1966. Statistics of atomic frequency standards. Proc. IEEE 54, 221–231.

Baldocchi, D.D., 2003. Assessing the eddy-covariance technique for evaluating the carbon dioxide exchange rates of ecosystems; past, present and future. Glob. Change Biol. 9, 479–492.

Buck, A., 1981. New equations for computing vapor pressure and enhancement factor. J. Appl. Meteorol. 20, 1527–1532.

Burba, G.G., Verma, S.B., 2001. Prairie growth, PAR albedo and seasonal distribution of energy fluxes. Agric. For. Meteorol. 107, 227–240.

Clark, K.L., Gholz, H.L., Moncrieff, J.B., Cropley, F., Loescher, H.W., 1999. Environmental controls over net exchanges of carbon dioxide from contrasting Florida ecosystems. Ecol. Apps. 9, 936–948.

Gash, J.H.C., Dolman, A.J., 2003. Sonic anemometer (co)sine response and flux measurement. I. The potential for (co)sine error to affect sonic anemometer-based flux measurements. Agric. For. Meteorol. 119, 195–207.

Goulden, M.L., Munger, J.W., Fan, S.-M., Daube, B.C., Wofsy, S.C., 1996. Measurements of carbon sequestration by long-term eddy covariance: methods and a critical evaluation of accuracy. Glob. Change Biol. 2, 169–182.

Fleagle, R.G., Businger, J.A., 1980. Introduction to Atmospheric Physics. Academic Press Inc., NY, 432 pp.

Foken, T., Wichura, B., 1996. Tools for quality assessment of surface-based flux measurements. Agric. For. Meteorol. 78, 83–105.

Foken, T., Oncley, S., 1995. Results of the workshop 'Instrumental and Methodical Problems of Land Surface Measurements'. Bull. Am. Meteorol. Soc. 76, 1191–1193.

Hollinger, D.Y., Aber, J., Dail, B., Davidson, E.A., Goltz, S.M., Hughes, H., Leclerc, M., Lee, T.J., Richardson, A.D., Rodrigues, C., Scott, N.A., Varier, D., Walsh, J. Spatial and temporal variability in forest-atmosphere CO_2 exchange. Glob. Change Biol., in press.

Kaimal, J.C., Finnigan, J.S., 1994. Atmospheric Boundary-Layer Flows; Their Structure and Measurement. Oxford University Press, UK, 453 pp.

Kaimal, J.C., Gaynor, J.E., Zimmerman, H.A., Zimmerman, G.A., 1990. Minimizing flow distortion errors in a sonic anemometer. Boundary Layer Meteorol. 53, 103–115.

Kaimal, J.C., Gaynor, J.E., 1991. Another look at sonic anemometry. Boundary Layer Meteorol. 56, 401–410.

Katul, G.G., Goltz, S.M., Hsieh, C.I., Cheng, Y., Mowry, F., Sigmon, J., 1995. Estimation of surface heat and momentum fluxes using the flux-variance method above uniform and non-uniform terrain. Boundary Layer Meteorol. 74, 237–260.

Katul, G.G., Hsieh, C.I., Bowling, D., Clark, K., Shurpali, N., Turnipseed, A., Albertson, J., Tu, K., Hollinger, D.Y., Evans, B., Offerle, B., Anderson, D., Ellsworth, D., Vogel, C., Oren, R., 1999. Spatial variability of turbulent fluxes in the roughness sublayer of an even-aged pine forest. Boundary Layer Meteorol. 93, 1–28.

Kristensen, L., Mann, J., Oncley, S.P., Wyngaard, J.C., 1997. How close is close enough when measuring scalar fluxes with displaced sensors? J. Atmos. Ocean. Tech. 14, 814–821.

Law, B.E., Kelliher, F.M., Baldocchi, D.D., Anthoni, P.M., Irvine, J., Moore, D., Van Tuyl, S., 2001. Spatial and temporal variation in respiration in a young ponderosa pine forest during a summer drought. Agric. For. Meteorol. 110, 27–43.

Lee, X., Finnigan, J., Paw, U.K.T., 2004. Coordinate systems and flux bias error. In: Lee, X., Massman, W., Law, B. (Eds.), Handbook of Micrometeorology, A Guide for Surface Flux Measurement and Analysis. Kluwer Press, Netherlands, 250 pp.

Lee, X., 1998. On micrometeorological observations of surface-air exchange over tall vegetation. Agric. For. Meteorol. 100, 1–11.

Loescher, H.W., Law, B.E., Mahrt, L., Hollinger, D.Y., Styles, J.M., Wofsy, S.C. Uncertainties in- and interpretation of carbon flux estimates using the eddy covariance technique. J. Geophys. Res., submitted for publication.

Loescher, H.W., Oberbauer, S.F., Gholz, H.L., Clark, D.B., 2003. Environmental controls on net ecosystem-level carbon exchange and productivity in a Central American tropical wet forest. Glob. Change Biol. 9, 396–412.

Luening, R., 2004. Measurements of trace gas fluxes in the atmosphere using eddy covariance: WPL corrections revisited. In: Lee, X., Massman, W., Law, B. (Eds.), Handbook of Micrometeorology, A Guide for Surface Flux Measurement and Analysis. Kluwer Press, Netherlands, 250 pp.

Liu, H., Peters, G., Foken, T., 2001. New equations for sonic temperature variance and buoyancy heat flux with an omnidirectional sonic anemometer. Boundary Layer Meteorol. 100, 459–468.

Mahrt, L., Lee, X., Black, A., Nuemann, H., Staebler, R.M., 2000. Nocturnal mixing in a forest subcanopy. Agric. For. Meteorol. 101, 67–78.

Massman, W., 2004. Concerning the measurement of atmospheric trace gas fluxes with open- and closed path eddy covariance system, the WPL terms and spectral attenuation. In: Lee, X., Massman, W., Law, B. (Eds.), Handbook of Micrometeorology, A Guide for Surface Flux Measurement and Analysis. Kluwer Press, Netherlands, 250 pp.

Moncrieff, J.B., Malhi, Y., Leuning, R., 1996. The propagation or errors in long-term measurements of land–atmosphere fluxes of carbon and water. Global Change Biol. 2, 231–240.

Paw, U.K.T., Baldocchi, D.D., Meyers, T.P., Wilson, K.B., 2000. Corrections of eddy covariance measurements incorporating both advective effects and density fluxes. Boundary Layer Meteorol. 97, 487–511.

Shimizu, T., Suzuki, M., Shimizu, A., 1999. Examination of the correction procedure for the flow attenuation in orthogonal sonic anemometers. Boundary Layer Meteorol. 93, 227–236.

Schotanus, P., Nieuwstadt, F.T.M., de Bruin, H.A.R., 1983. Temperature measurement with a sonic anemometer and its application to heat and moisture fluxes. Boundary Layer Meteorol. 26, 81–93.

Van der Molen, M.K., Gash, J.H.C., Elbers, J.A., 2004. Sonic anemometer (co)sine response and flux measurement. II. The effect of introducing an angle of attack dependent calibration. Agric. For. Meteorol. 122, 95–109.

Werle, P., Mucke, R., Slemr, F., 1993. The limits of signal averaging in atmospheric trace-gas monitoring by tunable diode-laser absorption spectroscopy (TDLAS). Appl. Phys. B57, 131–139.

Wieser, A., Fielder, F., Corsmeier, U., 2001. Influence of sensor design on wind measurements with sonic anemometer systems. J. Atmos. Ocean. Tech. 18, 1585–1608.

Wilczak, J.M., Oncley, S.P., Stage, S.A., 2001. Sonic anemometer tilt correction algorithms. Boundary Layer Meteorol. 99, 127–150.

Wyngaard, J.C., Zhang, S.-F., 1985. Transducer-shadow effects on turbulence spectra measured by sonic anemometers. J. Atmos. Ocean. Tech. 2, 548–558.